

Self-consistent Thomas-Fermi calculation of potential and current distributions in a two-dimensional Hall bar geometry

J. H. Oh and Rolf R. Gerhardt

Max-Planck-Institut für Festkörperforschung, Heisenbergstrasse 1, D-70569 Stuttgart, Federal Republic of Germany

(Received 1 May 1997)

The electrostatics of a two-dimensional, in-plane-gate-defined Hall bar is investigated by imposing the electrochemical equilibrium within the Thomas-Fermi approximation. We calculate the electrostatic potential self-consistently with the electron distribution and examine associated magnetic-field-induced compressible and incompressible regions as a function of temperature, bare screening length, and gate voltage with and without nondissipative currents. We find that the widths of the incompressible and compressible regions depend strongly on temperature and bare screening length. At very low temperature and small screening length, our results agree with an analytical work by Chklovskii, Matveev, and Shklovskii. For a small current applied on the Hall bar, the electron distribution is found to be slightly deformed while the width of the incompressible regions is not changed. Neglecting diamagnetic currents, we find that the current densities are distributed over the whole region occupied by electrons. [S0163-1829(97)06343-1]

I. INTRODUCTION

The local potential and current distributions of the two-dimensional electron gas (2DEG) in a Hall bar have been the subject of intense study because they are key factors in understanding the quantum Hall effect.¹⁻⁴ In the presence of a perpendicular magnetic field, the local potential of the 2DEG is determined by the peculiar screening properties of the electron system combined with the bare confinement potential of the Hall bar. Within the Thomas-Fermi approximation and at very low temperature, the area occupied by the 2DEG can be divided to two types of regions, compressible and incompressible regions. Due to the bare confinement potential of the Hall bar, there are “compressible” regions where a Landau level is pinned at the chemical potential. In these regions, electrons show a perfect screening, because they can be easily redistributed, and the potential is nearly flat. In the “incompressible” regions, where the chemical potential lies in the gap between two successive Landau levels, electrons do not contribute to screening because a redistribution is energetically impossible. In these regions the electron density is constant while the potential exhibits a large variation.

Various experimental attempts to measure the compressible and incompressible regions in the Hall bar have been made.⁵⁻⁷ Knott *et al.*,⁸ imaged the local potential distributions of the 2DEG induced by currents with a scanning polarization optical microscope based on the linear electro-optical effect. They found that the potential profile shows nonlinear behavior in the range of the quantum Hall plateau whereas it is usually linear. On the other hand, Ernst *et al.*⁹ examined edge channels of the Hall bar using magnetoplasmons which can be excited with a short voltage pulse. By time-resolved observation of the pulse propagation, they found three edge magnetoplasmon modes, which can be well described in terms of a finite width of the compressible regions near the edges. However, for a better understanding of the experimental results, it is necessary to know the detailed potential and electron density distribution in the Hall bar.

In this paper we study the local potential and current distributions of a two-dimensional electron gas in a narrow wire structure under a strong magnetic field within the Thomas-Fermi approximation. Chklovskii, Matveev, and Shklovskii¹⁰ (CMS) examined the formation of the edge channels and associated potential distribution for this structure and presented analytic expressions for the electrostatics. In their “electrostatic approximation”¹⁰ they used plausible *ad hoc* assumptions for the electrostatic boundary conditions. Specifically, they *assumed* perfect screening, leading to a constant electrostatic potential, within the two-dimensional electron system even in the absence of a magnetic field. Furthermore, they *assumed* that the resulting electron density profile $n_s(x)$ is changed by a strong magnetic field only near positions of integer filling factors, where “incompressible” regions with constant $n_s(x)$ occur. In a self-consistent theory of electrochemical equilibrium,³ on the other hand, the electron density profile is uniquely determined by the electrostatic potential and vice versa, and no *ad hoc* assumptions are necessary. In such a theory, the screening of electrons depends on the presence of the magnetic field and temperature as well as the bare two-dimensional screening length, as has been shown by Wulf *et al.*¹¹ within a Hartree calculation.

The purpose of the present work is twofold. First, we extend the CMS approach to more realistic situations such as finite temperature and finite screening length, and we require electrochemical equilibrium. To keep the calculations simple, we determine the electron distribution for a given electrostatic potential within the Thomas-Fermi approximation and follow the ideas of CMS to calculate the electrostatic potential for given charge distribution. We also examine the effect of in-plane gate voltages on the position of incompressible regions in accordance with a recent experimental investigation.¹² Second, we apply a nondissipative current, and investigate the change of the potential, charge, and current distributions by employing a generalized equilibrium density operator. The understanding of the current distribution in a Hall bar is still controversial. Chang¹³ stated that a current can flow only along the incompressible regions

because in a compressible region the electrostatic potential is flat and, therefore, a drift velocity of electrons is identically zero. On the other hand, according to the numerical results obtained by Pfannkuche and Hajdu,⁴ the equilibrium current is distributed over the whole sample rather than only in a localized region. Under the picture of the Landauer-Büttiker transport theory¹⁴ where both ends of the Hall bar are in contact with reservoirs at slightly different electrochemical potential, the nonequilibrium current is predicted to be in the compressible regions by Beenakker.¹⁵

The combination of the Thomas-Fermi approximation with analytic treatment of the electrostatics of a geometry with in-plane gates is close in spirit to a calculation in Ref. 3, where the 2DEG occupying a half plane was considered. Here we want to investigate the effect of a gate voltage across and a net current along a Hall bar geometry and therefore consider the 2DEG in a narrow wire confined by two in-plane gates. In Sec. II, we solve the electrostatics for a two-dimensional electron gas which is contained in a gate-defined Hall bar. Within the Thomas-Fermi approximation, the charge density is expressed in terms of the potential and the applied current by employing a generalized equilibrium density operator. In the case of zero current, our self-consistent potential and charge distributions are discussed in Sec. III and compared with those of CMS. In Sec. IV, we present results for the compressible and incompressible regions when a nondissipative current is applied. A brief summary is given in Sec. V.

II. FORMULATION OF ELECTROSTATICS

We consider a two-dimensional split-gate structure realized on the interface between two semiconductors which occupy the half spaces $z > 0$ and $z < 0$ with dielectric constants $\kappa_>$ and $\kappa_<$, respectively. Two semi-infinite metal gates extended at $x < -d$ and $x > d$ with constant potentials V_L and V_R , respectively, define the Hall bar along the y direction on the interface (x - y plane). We assume that electrons are distributed on the Hall bar together with a uniform positive background in the presence of a magnetic field applied along the z direction. Then, the charge density is only a function of x and z and has a form $\rho(x)\delta(z)$. The surface charge density $\rho(x)$ is expressed as,

$$\rho(x) = e[n_0 - n_s(x)], \quad (1)$$

where $n_s(x)$ and n_0 are surface densities of electrons and positively charged particles, respectively. Although our Hall bar is symmetric about $x=0$, an asymmetric charge density $\rho(x)$ can be obtained by applying a gate voltage $V_L - V_R \neq 0$ between the metal gates.

Since our system has translational invariance along the y direction, the electrostatic potential $V(x, z)$ is determined by a two-dimensional Laplace equation in the x - z plane with suitable boundary conditions. Two kinds of the boundary conditions are imposed on the electrostatic potential in our system. First, the electrostatic potential should be V_L and V_R , respectively, in the regions of the metal gates. Second, inside the Hall bar, the normal derivative of the electrostatic potential should be given by the surface charge density $\rho(x)$. Since the two boundary conditions are independent of each other, we can treat them separately and write down the elec-

trostatic potential in the form of $V(x, z) = V_1(x, z) + V_2(x, z)$ where V_1 and V_2 satisfy simpler boundary conditions.

The potential $V_1(x, z)$ is restricted only by the boundary values of V_L and V_R in each gate region,

$$V_1(x, z=0) = \begin{cases} V_L, & x < -d \\ V_R, & x > d, \end{cases} \quad (2)$$

and, otherwise, satisfies the two-dimensional Laplace equation. The solution of $V_1(x, z)$ can be found by the conventional theory of analytic functions,¹⁶

$$V_1(x, z) = V_R + \frac{V_L - V_R}{\pi} \text{Im} \ln \left\{ \frac{\zeta}{d} - \sqrt{\zeta^2/d^2 - 1} \right\}, \quad (3)$$

with a complex variable $\zeta = x + iz$. For $|x| < d$ and $z = 0$ one finds from Eq. (3),

$$V_1(x) = \frac{V_R + V_L}{2} - \frac{V_L - V_R}{\pi} \arcsin(x/d). \quad (4)$$

As one can expect, different gate potentials $V_R \neq V_L$ give rise to an asymmetric potential distribution. Otherwise, the potential $V_1(x, z)$ is constant all over the space.

The potential $V_2(x, z)$ depends on the boundary condition resulting from the displacement field of the charge density $\rho(x)$, i.e., for $|x| < d$,

$$\kappa_> \frac{\partial V_2}{\partial z}(x, z=0^+) - \kappa_< \frac{\partial V_2}{\partial z}(x, z=-0^+) = -4\pi\rho(x), \quad (5)$$

and satisfies $V_2(x, 0) = 0$ for $|x| > d$. Using the conventional theory of analytic functions, $V_2(x, z)$ can be represented as the imaginary part of a holomorphic function F in the complex plane, $V_2(x, z) = \text{Im}F(\zeta)$. Since $\partial V_2/\partial x = \text{Im}dF/d\zeta$ and $\partial V_2/\partial z = \text{Re}dF/d\zeta$, $F(\zeta)$ satisfies the following boundary conditions:

$$\begin{aligned} \text{Re} \frac{dF}{d\zeta} \Big|_{\zeta=x+i0^+} &= r(x), \quad \text{for } |x| < d \\ \text{Im} \frac{dF}{d\zeta} \Big|_{\zeta=x+i0^+} &= 0, \quad \text{for } |x| > d, \end{aligned} \quad (6)$$

where $r(x) = -4\pi\rho(x)/(\kappa_> + \kappa_<)$ and $\partial V_2(x, -0^+)/\partial z = -\partial V_2(x, 0^+)/\partial z$ has been anticipated. The above boundary conditions define the discontinuity of the imaginary part of the auxiliary function,

$$h(\zeta) = i\sqrt{d^2 - \zeta^2} \frac{\partial F}{\partial \zeta} \quad (7)$$

along the real axis and give rise to

$$\text{Im}h(x+i0^+) = \begin{cases} r(x)\sqrt{d^2 - x^2} & \text{for } |x| < d \\ 0 & \text{for } |x| > d, \end{cases} \quad (8)$$

where $\sqrt{d^2 - \zeta^2}$ is holomorphic, except for the branch cut, ($|x| > d$). Then, in all of space, $h(\zeta)$ can be obtained using the Schwartz integral as

$$\begin{aligned}
h(\zeta) &= \frac{1}{\pi} \int_{-\infty}^{\infty} dx \frac{\text{Im}h(x+i0^+)}{x-\zeta} + c \\
&= \frac{1}{\pi} \int_{-d}^d dx \frac{r(x)\sqrt{d^2-x^2}}{x-\zeta} + c, \quad (9)
\end{aligned}$$

with a real constant of integration c . Then, the solution of $V_2(x)$ is found from Eq. (9) by straightforward integration,

$$V_2(x) = -\frac{1}{\pi} \int_{-d}^d dt r(t) K(x, t),$$

$$K(x, t) = \ln \left| \frac{\sqrt{(d^2-x^2)(d^2-t^2)} + d^2 - tx}{(x-t)d} \right|. \quad (10)$$

For a given charge density $\rho(x)$, the potential $V_2(x)$ is uniquely determined by Eq. (10). For an arbitrary charge density $\rho(x)$, we find that Eq. (10) cannot be evaluated analytically. We use a numerical method to obtain $V_2(x)$ in this work.

Since our system is ideal and no dissipation occurs, the surface electron density $n_s(x)$ is obtained from the equilibrium density operator $\hat{\rho}$ through the relation,

$$n_s(x) = \text{Tr}[\delta(x-\hat{x})\hat{\rho}], \quad (11)$$

where Tr means the sum over all diagonal matrix elements. Here, the equilibrium density operator $\hat{\rho}$ is given by maximizing the entropy of the system, taking into account all additive conserved quantities: the total energy, the number of electrons, and the total momentum of electrons in the y direction. In a strong perpendicular magnetic field B , the matrix elements in Eq. (11) are easily evaluated. If the electrostatic potential $V(x)$ varies smoothly in the plane of the 2DEG, i.e., on a characteristic length much larger than the magnetic length $l_m = \sqrt{\hbar/eB}$, the spatial extent of the wave functions can be neglected on the scale d and the Hartree approximation for evaluating Eq. (11) reduces to the Thomas-Fermi approximation. Then, the electron density $n_s(x)$ is related to the total potential energy of an electron, $U(x) = U_1(x) + U_2(x) = -e[V_1(x) + V_2(x)]$ through the relation,⁴

$$n_s(x) = \int dE D(E) f\{[E + U(x) - \hbar v x / l_m^2 - \mu] / k_B T\}, \quad (12)$$

with $f(\epsilon) = 1/[1 + \exp(\epsilon)]$ the Fermi function, μ the electrochemical potential, and T the temperature. Here, $D(E)$ represents the two-dimensional density of states, $D(E) = (g_s/2\pi l_m^2) \sum_{j=0}^{\infty} \delta\{E - \hbar \omega_c(j+1/2)\}$ where $g_s=2$ takes into account the spin degeneracy and $\omega_c = eB/m^*$ the cyclotron frequency. The quantity $\hbar v x / l_m^2$ represents a kinetic energy of the drift motion at each point and depends linearly on x because a Landau level centered at $x=x_0$ has a momentum of $\hbar x_0 / l_m^2$. The parameter v is fixed by the total current in the y direction, $I = 2e\bar{n}vd$ where \bar{n} is the average electron density in the Hall bar,

$$\bar{n} = \frac{1}{2d} \int_{-d}^d n_s(x) dx. \quad (13)$$

According to Eq. (12), the electron density $n_s(x)$ at a position x depends on the electrostatic potential only at that position. This fact leads to a simple real-space picture of screening at very low temperature.

When electrons are completely depleted in the Hall bar, i.e., $n_s(x)=0$, we can find the electrostatic potential energy analytically from Eq. (10);

$$U_2(x) = -eV_2(x) = -E_0 \sqrt{1-x^2/d^2}, \quad (14)$$

where $E_0 = 4\pi e^2 n_0 d / (\kappa_> + \kappa_<)$ is a pinch-off energy. This potential results from the positive background and has an elliptic shape with the minimum value at $x=0$. The voltage difference between the gates serves to shift the minimum position of the electrostatic potential energy $U(x)$.

Once electrons start to occupy the Hall bar, the electrostatics depends on various parameters; applied current (I), magnetic fields (B), temperature (T), gate voltages (V_R, V_L), and average electron density (\bar{n}). Another important parameter is the two-dimensional screening length $a_0 = (\kappa_> + \kappa_<) / 4\pi e^2 D_0$, where $D_0 = m^* / \pi \hbar^2$ is the two-dimensional density of states without a magnetic field. For $\kappa_> = \kappa_<$, the two-dimensional screening length becomes $a_0 = a_B^* / 2$, with $a_B^* = \kappa_< \hbar^2 / e^2 m^*$ the effective Bohr radius. Since the chemical potential μ is directly related to the average electron density (\bar{n}), we investigate the electrostatics of the Hall bar for a given set of the above six parameters. The determination of $U(x)$ and $n_s(x)$ constitutes a self-consistent problem because the surface electron density $n_s(x)$ is uniquely determined from a electrostatic potential $U(x)$ by Eq. (12) while the electrostatic potential is given by Eq. (10). Using a numerical method, we solve the self-consistent problem exactly. In the following we measure length and energy in units of d and E_0 , respectively, and present calculated results in dimensionless parameters such as a_0/d and eV_R/E_0 . We choose an energy reference for our system as $V_L=0$ without a loss of generality. So, for the case of complete depletion of electrons, the minimum value of the electrostatic potential energy $U(x)$ is $-E_0$ at $V_R=0$.

III. POTENTIAL AND ELECTRON DISTRIBUTIONS WITHOUT A CURRENT

First, we discuss the calculated potential and electron distributions of the 2DEG in the Hall bar without an imposed current, i.e., the charge density is calculated in Eq. (12) with $v=0$. For solving the self-consistent problem we start with solutions of zero magnetic field at $T=0$.

A. Results for $B=0$ and $T=0$

For $B=0$ and $T=0$, the surface electron density is given as $n_s(x) = D_0 [E_F - U(x)] \theta[E_F - U(x)]$, where the Fermi energy is E_F and $\theta(x)$ the unit step function. Then, Eq. (10) reduces to the linear integral equation,

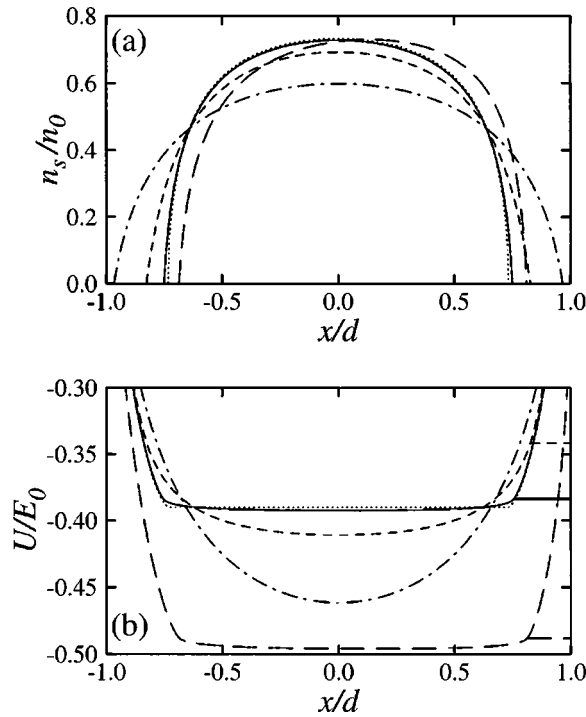


FIG. 1. The (a) electron densities $n_s(x)$ and (b) electrostatic potentials $U(x)$ at $B=0$ and $T=0$, are plotted for various bare screening length $a_0/d=0.5$ (dot-dashed), 0.1 (dashed), and 0.01 (solid). Here, the average electron density is $\bar{n}/n_0=0.458$ with $V_R=0.0$. The long-dashed lines represent the results with $V_R=0.2$. See the text for the dotted lines. In (b), the horizontal lines describe the corresponding values of the Fermi energy E_F .

$$U_2(x) = -E_0 \sqrt{1 - \frac{x^2}{d^2}} + \frac{1}{a_0} \int_{-b}^a [E_F - U(t)] K(x,t) dt, \quad (15)$$

where electrons are assumed to be distributed in the region $-b < x < a$. By writing $U(x)$ and $n_s(x)$ in units of E_0 and n_0 in Eq. (15), our problem depends on only dimensionless parameters a_0/d , eV_R/E_0 , and \bar{n}/n_0 . As shown in Eq. (14), the first term in Eq. (15) is the contribution of the positive background when electrons are completely depleted. As we increase the number of electrons, the second term of Eq. (15) becomes important in determining the potential profile and tends to flatten the potential shape due to the screening by electrons in the occupied region. However, the flatness depends on the two-dimensional screening length a_0 and the average electron density \bar{n} .

To examine effects of a_0 and \bar{n} on the electrostatics, we first consider zero gate voltage $V_R=0$. Then, one expects a symmetrical geometry with $a=b$. For given values of a_0/d and \bar{n}/n_0 , Eq. (15) determines the width $2b$ of the region occupied by electrons. With a typical value of $\bar{n}/n_0=0.458$, we compare the calculated potential $U(x)$ and electron density $n_s(x)$ in Fig. 1 for several values of a_0/d . The average electron density $\bar{n}/n_0=0.458$ is chosen to give a value of $b/d=0.75$ at $a_0/d=0.01$. The calculated potential $U(x)$ and electron density $n_s(x)$ demonstrate that the electrostatics depends crucially on the ratio a_0/d . When the bare screening length a_0 is comparable to d , the self-consistent potential

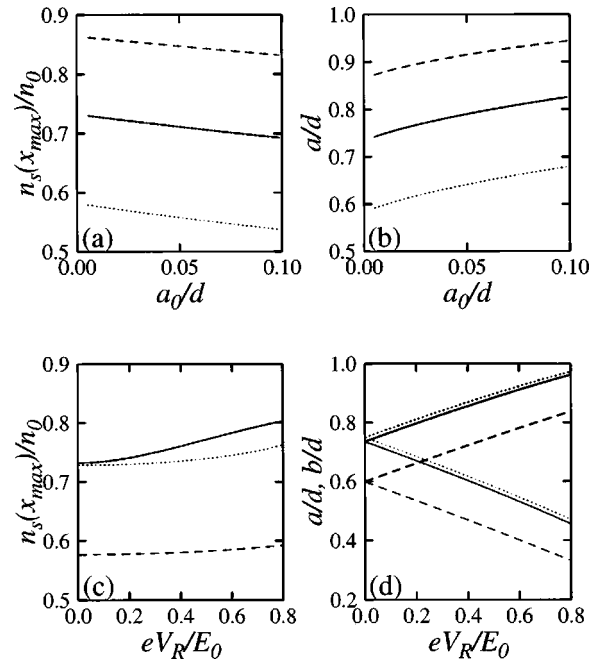


FIG. 2. (a) Maximum value of the electron density $n_s(x)$ and (b) half width of the region occupied by electrons a/d are depicted as a function of a_0/d for $\bar{n}/n_0=0.668$ (dashed), 0.458 (solid), and 0.279 (dotted) with $V_R=0$. Calculated results are compared as a function of V_R in (c) and (d) for different sets of the parameters $[\bar{n}/n_0, a_0/d]=[0.458, 0.001]$ (solid), $[0.458, 0.01]$ (dotted), and $[0.279, 0.01]$ (dashed). In (d), lines with a positive slope describe a/d .

exhibits a similar behavior to the potential of Eq. (14), where there is no screening due to a lack of electrons. The associated electron density is found to be distributed over a relatively broad region. However, as the ratio a_0/d becomes smaller, the potential becomes flatter in the region occupied by electrons, and the electron density is distributed over a narrower region because electrons screen the positive background more effectively. Eventually, in the limit of $a_0/d=0$, the self-consistent electron density is found to approach $n_s^0(x) = n_0 \sqrt{(b^2 - x^2)/(d^2 - x^2)}$ [the dotted line in Fig. 1(a)], which was obtained by CMS. The charge density $n_s^0(x)$ is a solution of the electrostatic problem, where $U(x)$ is assumed to be perfectly flat in the region $|x| < b$ as shown in Fig. 1(b).

For different values of the average electron density \bar{n} , we find a similar behavior for the electrostatics as a function of a_0/d . We show the maximum value of $n_s(x)$ and the half width of the region occupied by electrons, a/d , as a function of a_0/d in Fig. 2 (upper panel) for three different values of \bar{n}/n_0 . As the ratio a_0/d decreases, the screening by electrons becomes more effective, independently of \bar{n}/n_0 , leading to a larger maximum value of the electron density $n_s(x)$ and smaller a/d . When, for a fixed value of a_0/d , the average electron density \bar{n}/n_0 increases we find that the electron screening also becomes more effective and the electron density $n_s(x)$ is closer to $n_s^0(x)$. Thus, the electron density $n_s^0(x)$ obtained by CMS applies to a Hall bar with sufficiently large values of d/a_0 and \bar{n}/n_0 .

Now we consider a finite gate potential, $V_R \neq 0$, leading to an asymmetric electron distribution, i.e., $a \neq b$ in Eq. (15),

because electrons are redistributed to screen the potential difference between the gates. We find that the overall shape of the electron density is shifted from the case of $V_R=0$ and, therefore, the maximum value of the electron density $n_s(x)$ occurs away from $x=0$ (long-dashed lines in Fig. 1). However, the width of the region occupied by electrons, $(a+b)/d$ is nearly independent of V_R while the maximum value of the electron density $n_s(x)$ becomes larger with an increase of V_R for given average electron density \bar{n} and bare screening length a_0/d . In the lower panel of Fig. 2, we show the maximum value of $n_s(x)$, a/d , and b/d as a function of gate voltage V_R for several sets of \bar{n} and a_0/d . With a given average electron density $\bar{n}/n_0=0.458$, the maximum value of the electron density $n_s(x)$ with $a_0/d=0.001$ (solid) is found to increase more rapidly than with $a_0/d=0.01$ (dotted) as a function of gate voltage V_R . Comparing the dotted and dashed lines in Fig. 2(c), we find that the variation of the maximum value of $n_s(x)$ with increasing V_R shows the same increasing rate regardless of the average electron density \bar{n}/n_0 with a given value of a_0/d . The width of the region occupied by electrons $(a+b)/d$ is found to be nearly independent of V_R as can be easily seen from Fig. 2(d). This means that an asymmetric shape of the electron density causes the variation of its maximum value with varying gate voltage V_R . This fact is found to be responsible for the severe change of the electrostatic potential in the center of the Hall bar at finite magnetic field, as discussed in the following section.

B. Compressible and incompressible regions

For finite magnetic field and temperature, the self-consistent problem is now a nonlinear integral equation, and must be solved by a numerical iteration method. For this, starting with the self-consistent potential at $T=0$ and $B=0$, we first ‘‘heat’’ the electronic system sufficiently high and, then, cool it slowly to the desired temperature. At each temperature step we ensure fully converged results by employing the Newton-Raphson method to solve the nonlinear equation of Eqs. (10) and (12).

In the presence of a magnetic field, screening by electrons is drastically changed due to the δ -shaped density of states $D(E)$ in Eq. (12). According to Wulf *et al.*,¹¹ an effective screening length for finite magnetic field and temperature is given as

$$a_T = \frac{k_B T}{\hbar \omega_c} \frac{4}{p(2-p)} a_0, \quad (16)$$

where p is the filling factor ν_H modulo 2 and ν_H is the local filling factor defined as $\nu_H(x) = n_s(x)/n_L$, with a Landau level degeneracy $n_L = 1/2\pi l_m^2$. Thus, one expects a periodic change of the screening property as a function of the magnetic field. There is essentially no screening when the chemical potential μ lies in the gap between two successive Landau levels, i.e., $p=0$. Otherwise, i.e., when μ is pinned in a Landau level, electrons show a nearly perfect screening at a low temperature.

In this work, we express the magnetic field as the occupation number $\nu(0) \equiv n(0)/n_L$, where $n(0)$ is the maximum of the electron density, $n_s(x)|_{x=0}$ at $B=T=V_R=0$. For a

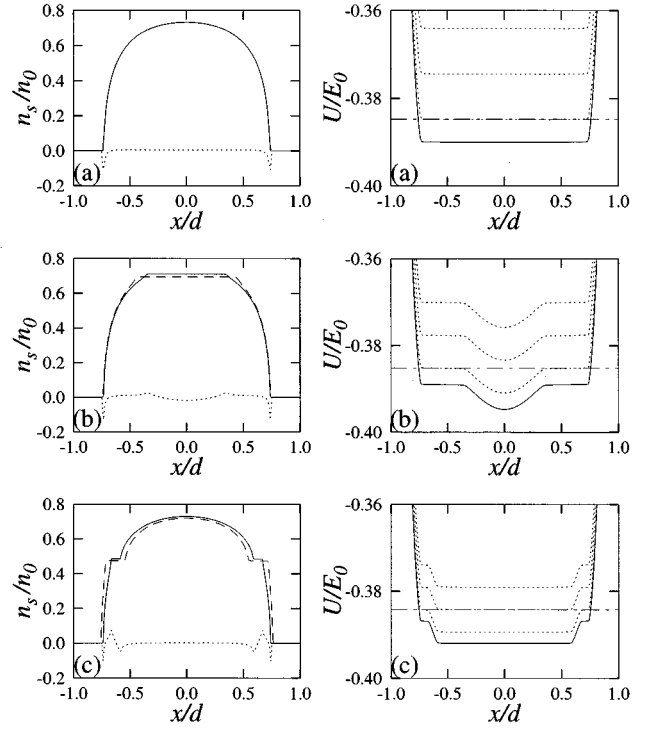


FIG. 3. For $\nu(0)=1.5$ (a), 2.05 (b), and 3.0 (c), we plot the electron densities $n_s(x)$ and electrostatic potentials $U(x)$ calculated with $V_R=0.0$, $k_B T/E_2=0.005$, $\bar{n}/n_0=0.458$, and $a_0/d=0.01$ [E_2 is equal to a cyclotron energy at the occupation number $\nu(0)=2.0$]. The dotted lines (left column) represent the difference between the electron densities with and without magnetic fields. The dashed and dotted lines (right column) describe the chemical potential and Landau levels, respectively. The electron densities $n_s(x)$ at $a_0/d=0.05$ are also shown with dashed lines.

given set of the parameters the occupation number is inversely proportional to the magnetic field and indicates the appearance of the incompressible region at $x=0$. We expect that at even integer values of $\nu(0)$ the chemical potential μ is about to drop into the gap between two successive Landau levels at $x=0$ ($T=0$) and, therefore, an incompressible region is about to be formed near $x=0$. To understand the effects of the magnetic field more easily, we first discuss results calculated for a very low temperature, $k_B T/E_2=0.005$ [E_2 is equal to a cyclotron energy at the occupation number $\nu(0)=2.0$]. The electrostatics at higher temperatures and its temperature dependence will be shown in a later paragraph.

Figure 3 shows the potentials and electron densities of the Hall bar calculated for several magnetic fields at low temperature. In Fig. 3(a), we plot the electron density $n_s(x)$ (left panel) and electrostatic potential energy $U(x)$ (right panel) at a very strong magnetic field or $\nu(0)=1.5$, where the chemical potential (dot-dashed line) is pinned at the lowest Landau level and the compressible region extends over the whole sample. In this case, a change in a screening ability due to the magnetic field is easily examined. According to CMS one should expect no change in the electron density $n_s(x)$ from the results for zero magnetic field, because a perfect screening is assumed even for zero magnetic field. In our case, however, the calculated electron density $n_s(x)$ shows a slight difference depending on the presence of the magnetic

field. The dotted line in the left panel of Fig. 3 shows the difference between the electron densities with and without magnetic field at the same temperature. In the presence of the magnetic field, we find that electrons are distributed over smaller region and, therefore, the maximum of the electron density increases slightly. This means that the screening by electrons is more effective due to the magnetic field, as expected by Eq. (16). The potentials (solid lines in the right panel) also become flatter in the presence of the magnetic field.

As the occupation number $\nu(0)$ in the center increases, or the magnetic field is reduced from the case of Fig. 3(a), a flat region in the electron density starts to appear in the center of the Hall bar because the chemical potential there is about to lie between the first and second Landau levels. Whereas the first appearance of the flat region for zero temperature is expected at $\nu(0)=2.0$, we find that it starts at about $\nu(0)=1.99$ due to the finite temperature. Figure 3(b) shows the results at $\nu(0)=2.03$, where the chemical potential (dot-dashed line) lies in the gap between two Landau levels around the center of the Hall bar. As a result, we find an incompressible region, where the electron density is constant and the local filling factor $\nu_H(x)$ has an integer value, around the center of the Hall bar. The potential shows a large spatial variation, of about $\hbar\omega_c$, due to a lack of a screening in the incompressible region. By increasing the occupation number $\nu(0)$ further, the central incompressible region becomes larger until the chemical potential touches the upper unoccupied Landau level and, then, is divided into two regions by the appearance of another compressible region, in the center. Figure 3(c) shows the result at $\nu(0)=3.0$, where a central compressible region is bounded by two incompressible regions.

In the left column of Fig. 3, we also show the electron density (dashed lines) for the larger value of $a_0/d=0.05$. To compare the results with the case of $a_0/d=0.01$, the occupation number $\nu(0)=n(0)/n_L$ is defined with the electron density $n(0)=n_s(x)|_{x=0}$ at $a_0/d=0.05$. So, we expect a similar formation of compressible and incompressible regions. At $\nu(0)=1.5$, we find the same result as for the case of $a_0/d=0.01$ because the screening of electrons is perfect all over the region. However, at other values of $\nu(0)$, the compressible and incompressible regions have different widths from the case of $a_0/d=0.01$; As the ratio a_0/d becomes larger, the calculated width of the incompressible region increases at the same occupation number while that of the compressible region decreases.

In Fig. 4(a), we show the position of the incompressible regions for different values of $\nu(0)$, where the same parameters as in Fig. 3 are used. The dotted lines represent the boundaries predicted by CMS. The incompressible regions start to appear at about $\nu(0)=2.0$ and 4.0 at the center of the Hall bar and become larger as $\nu(0)$ increases. Then, eventually, they split into two incompressible regions which move to the edges as $\nu(0)$ increases. This behavior is in good agreement with that obtained by CMS around $\nu(0)=2.0$ and 4.0 , i.e., around the center of the Hall bar [as shown Fig. 4(a)], despite the finite temperature used in our calculation. Near the edges, however, our results for the boundaries of the incompressible regions disagree with the prediction of CMS with respect to both their positions and their widths.

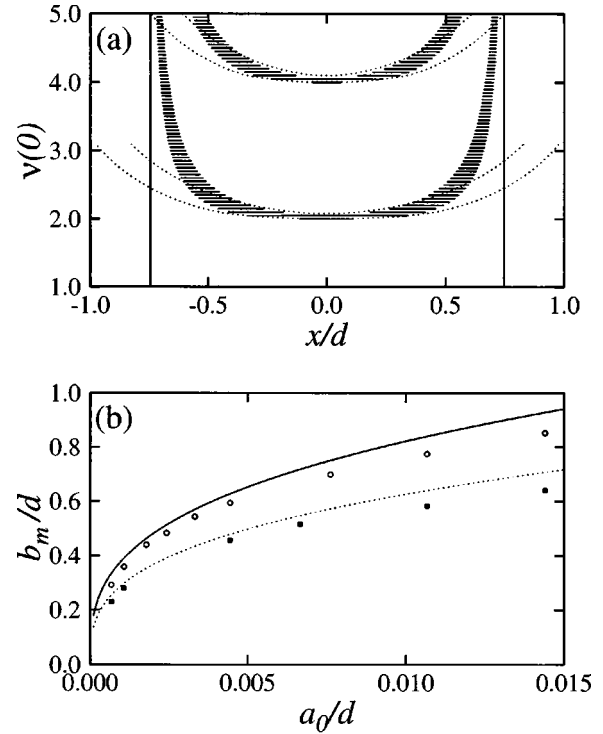


FIG. 4. (a) Incompressible regions with parameters as in Fig. 3, drawn in the $\nu(0)$ -coordinate space. The dotted lines show boundaries predicted by CMS. (b) Maximum width of the incompressible strip around $\nu(0)=2.0$ as a function of a_0/d for $\bar{n}/n_0=0.458$ (circle) and 0.279 (square). The solid and dotted lines describe results obtained by CMS for each average density \bar{n}/n_0 .

This discrepancy results from the oversimplified assumption of CMS that the central compressible region is narrower than two adjacent incompressible regions. This assumption also gives rise to a different maximum width of the central incompressible region from ours. In Fig. 4(b), we calculate maximum widths of the central incompressible region around $\nu(0)=2.0$ as a function of a_0/d for $\bar{n}/n_0=0.458$ (solid) and 0.279 (dotted). According to the approach by CMS, the maximum width of the central incompressible strip is proportional to $(a_0/d)^{1/3}$. In our case, the calculated results at $T=0$ are obtained by a linear extrapolation method from values at finite temperature, and exhibit a similar behavior as a function of a_0/d . However, our calculated results show smaller values than those by CMS over the whole range of a_0/d for both $\bar{n}/n_0=0.458$ and 0.279 .

For an asymmetric case $V_R \neq 0$, the width of the incompressible region also depends on the gate potential V_R . We show typical results for the electron density $n_s(x)$ and the electrostatic potential $U(x)$ at $V_R=0.2$ in Figs. 5(a) and 5(b), respectively. Compared to the result at $V_R=0$, the electron density is shifted with a slightly changed width of the incompressible regions, and the electrostatic potential exhibits a strongly asymmetric shape. As we vary the gate voltage V_R , a drastic change is found in the central incompressible regions, which is related to the maximum value of the electron density $n_s(x)$. As already shown in Fig. 2, the maximum value of the electron density increases with an increase of the gate voltage. Thus, for a given magnetic field, the ratio of the maximum electron density to the Landau level degeneracy

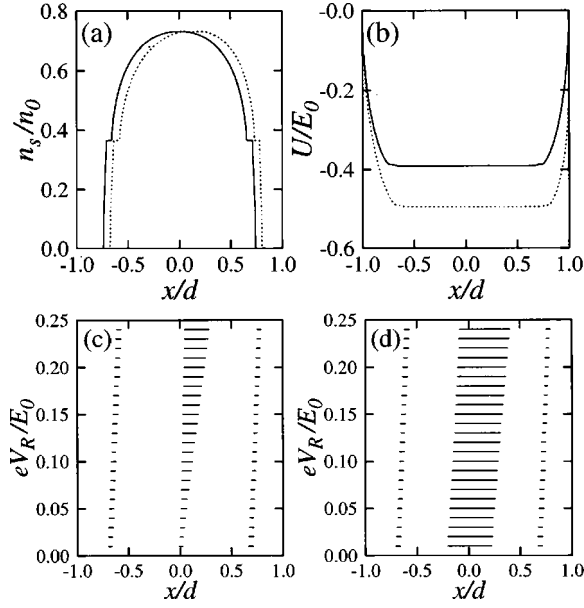


FIG. 5. For $\nu(0)=3.99$, (a) the electron densities $n_s(x)$ and (b) electrostatic potentials $U(x)$ are compared at $V_R=0$ (solid) and 0.2 (dotted). We also show the incompressible regions in the V_R -coordinate space for the occupation numbers $\nu(0)=3.99$ (c) and 4.035 (d). The parameters used are $a_0/d=0.01$, $k_B T/E_2=0.005$, and $\bar{n}/n_0=0.458$.

n_L or effective occupation number $\nu(0)$ becomes larger as the gate voltage V_R increases. Figures 5(c) and 5(d) show the position of incompressible regions in the V_R versus x -coordinate diagram, at occupation numbers $\nu(0)=3.99$ and 4.035, respectively. We find that the incompressible regions increase as the gate voltage becomes larger.

Now we discuss the effect of temperature on the electrostatic potential energy $U(x)$ and electron distribution $n_s(x)$. According to Eq. (16), the screening length increases linearly with increasing temperature, because electrons can be redistributed by a thermal excitation to unoccupied Landau levels. Thus, one expects that the potential becomes less flat in the compressible regions. Numerically, we examine the temperature dependence of the electrostatics for various sets of the parameters V_R , \bar{n} , a_0 , and $\nu(0)$. A typical result for self-consistent potential and corresponding electron density is shown in Fig. 6 for $V_R=0$, $\bar{n}=0.458$, and $a_0/d=0.01$. Note that the electrostatic potential energy is expressed in units of E_2 for easy comparison. The magnetic field is chosen to yield $\nu(0)=4.035$, where an incompressible strip is formed at the center as well as near the edges. With an increase of temperature, the slope of the potential in the compressible region is found to increase proportional to temperature $k_B T$, because the screening by electrons becomes less effective. On the other hand, the width of the incompressible region is found to decrease linearly with increasing temperature. As a result, the potential distribution shows strongly changed shapes. A drastic change of the electrostatic potential due to the temperature is found around the boundaries of the central incompressible region, at $x/d \sim \pm 0.3$ in Fig. 6(a). There, as the temperature is varied from $k_B T/E_2=0.005$ to 0.5, the change of the potential distribution is an order of $\hbar\omega_c$ at $x/d \sim \pm 0.3$. In addition, a similar potential variation occurs

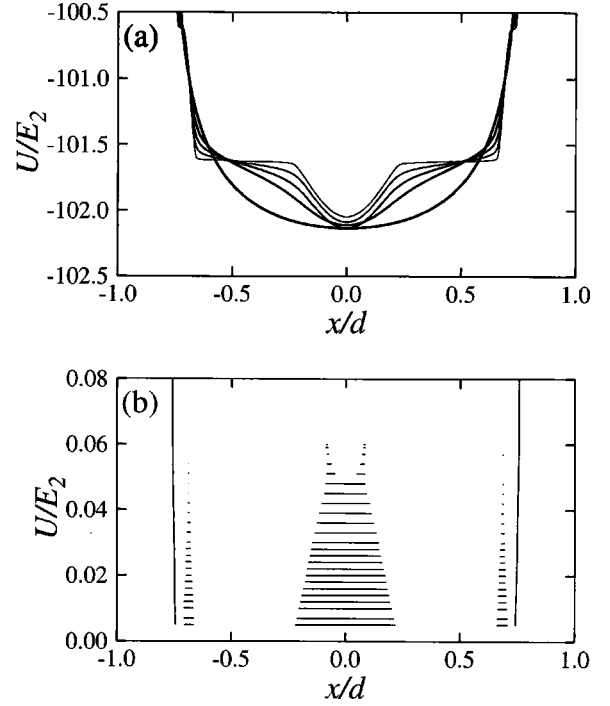


FIG. 6. (a) The electrostatic potentials $U(x)$ in units of E_2 plotted for temperatures $k_B T/\hbar\omega_c=0.005, 0.01, 0.06, 0.1$, and 0.5 with $\nu(0)=4.035$, $a_0/d=0.01$, $\bar{n}/n_0=0.458$, and $V_R=0.0$. A thicker solid line describes a higher temperature. (b) The incompressible region in the temperature-coordinate space.

over a relatively wide region of the Hall bar. Thus, we expect that this potential variation with respect to the temperature can be measured experimentally using the scanning polarization optical microscope.^{5,8}

In Fig. 6(b), we show evolutions of the incompressible region in the temperature versus the x -coordinate diagram. At very low temperatures, the width of the incompressible regions is found to vary linearly with the temperature. Based on this fact, we use the results at finite temperatures to obtain the width of the central incompressible region at $T=0$ in Fig. 4(b) by interpolating linearly. As the temperature increases, the central incompressible strip becomes smaller more rapidly than those at edges and, eventually, splits into two parts. This splitting of the incompressible region is caused by a thermal excitation of electrons. The temperature at which the first splitting occurs depends on the energy difference $\Delta(x)$ between the chemical potential μ and the lowest unoccupied Landau level. Since, for $V_R=0$, the electrostatic potential has a minimum value at $x=0$ in the central incompressible region, $\Delta(x)$ has the smallest value at that point and the first appearance of the splitting occurs there. The temperature dependence of the local filling factor ν_H in the incompressible region follows from Eq. (12);

$$\nu_H(x) = k + \frac{1}{1 + \exp[\Delta(x)/k_B T]}, \quad (17)$$

where k is the number of occupied Landau levels. Even though the energy difference $\Delta(x)$ also depends on the temperature, our calculated result fits well to the above equation with a constant $\Delta(x)$, especially at the point of the maximum electron density ($x=0$).

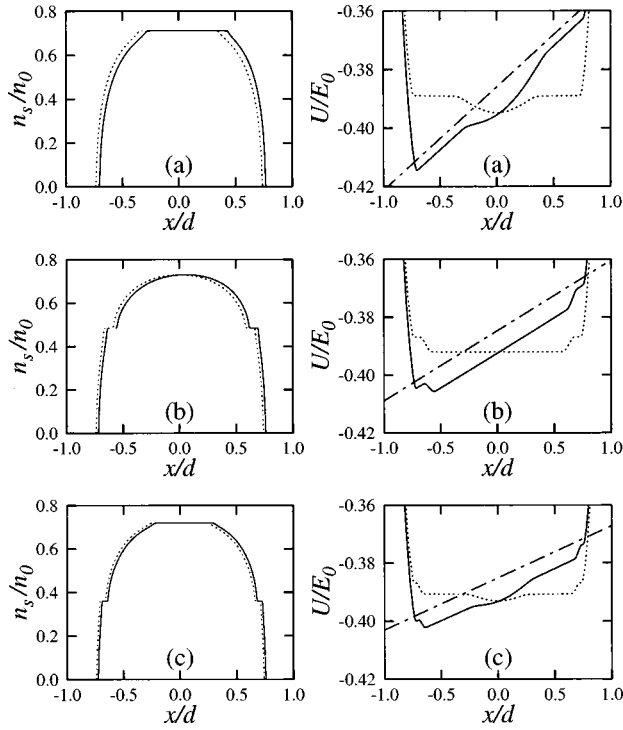


FIG. 7. For occupation numbers $\nu(0)=2.05$ (a), 3.0 (b), and 4.05 (c), the calculated electron densities and potential distributions are drawn when small drift velocity $v=0.2v_{0y}$ (solid) is imposed, and compared with results for $v=0$ (dotted line). Parameters used are $k_B T/E_2=0.005$, $a_0/d=0.01$, $\bar{n}/n_0=0.458$, and $V_R=0.0$. The dot-dashed lines (right column) represent the effective chemical potential $\mu(x)$.

For other sets of the parameters, we find behavior similar to the above results, although the width and position of the compressible and incompressible regions are different from case to case. For instance, as we decrease the ratio a_0/d keeping the other parameters as in Fig. 6, the maximum variation of the electrostatic potential with respect to the temperature occurs at a smaller point than $x/d \sim 0.3$, as already expected in Fig. 4. However, we find that the change of the potential distribution is still of order $\hbar\omega_c$ over the temperature change of $k_B T/E_2=0.5$.

IV. COMPRESSIBLE AND INCOMPRESSIBLE STRIPS UNDER FINITE CURRENT

Now we consider the Hall bar under a finite current, i.e., $v \neq 0$ in Eq. (12). In this case, the drift motion of electrons under magnetic field gives rise to an electric field $\vec{E}=(-vB, 0)$ which transfers electrons from one side of the Hall bar to the other. Thus, one expects an asymmetric charge density induced by the current even for the case of $V_L=V_R$. For a small drift velocity, $v=0.2v_0$ ($v_0=1/4\pi\hbar D_0 a_0$), the calculated potential $U(x)$ and electron density $n_s(x)$ are depicted in Fig. 7 with $a_0/d=0.01$, $\bar{n}/n_0=0.458$, and $k_B T/E_2=0.005$. At each occupation number, we compare the results with the case of zero current. The transfer of electrons leads to additional contributions to the potential distribution proportional to $\hbar vx/l_m^2$ as shown in the right column of Fig. 7. Thus, the resulting potential dis-

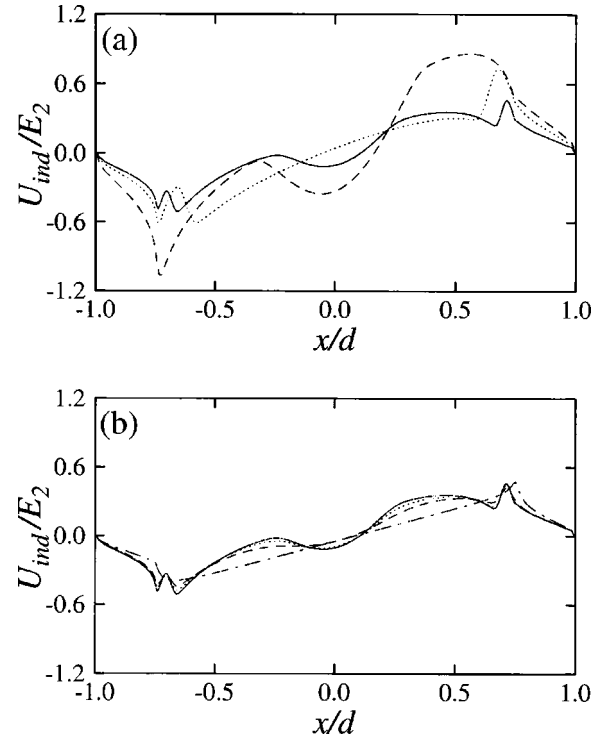


FIG. 8. The induced potentials by both current and magnetic field in units of E_2 are shown in (a) across the Hall bar for $\nu(0)=2.05$ (dashed), 3.0 (dotted), and 4.05 (solid) with the same parameters as in Fig. 7. In (b), the temperature dependence of the induced potential at $\nu(0)=4.05$ is shown for temperatures; $k_B T/E_2=0.005$ (solid), 0.06 (dotted), 0.1 (dashed), and 0.5 (dot-dashed).

tributions are drastically different from the case of zero current indicated by dotted lines. With this modified electrostatic potential, the electron density $n_s(x)$ is determined by an effective chemical potential $\mu(x)=\mu+\hbar vx/l_m^2$ (dot-dashed line), as shown in Eq. (12). The calculated electron density (solid line) is found to be shifted by the applied current, however, the overall shapes remain the same as in the case of zero current, as shown in the left column of Fig. 7.

An important effect of the applied current is that an energy difference between both edges develops, which is directly related to the Hall voltage. The Hall voltage is defined as the potential difference between energies of an injected and removed electron at each edge, respectively. We examine the Hall voltage (Hall-resistance) as a function of magnetic field, by calculating the potential difference between the two points where the effective chemical potential $\mu(x)$ is equal to the electrostatic potential $U(x)$. The obtained Hall resistance of our system does not show any plateau, but a linear behavior over the whole range of the magnetic fields. Using the Hartree approximation, Pfannkuche and Hajdu obtained structured behavior of the magnetoresistance, however, they also could not produce any quantized value.⁴

The induced potential by both current and magnetic field is found to show a strong position dependence. For several values of the magnetic field, the induced potentials are drawn in Fig. 8(a) with the same parameters as in Fig. 7. The charge transfer over the Hall bar causes additional peaks in the induced potential at about $x/d \sim \pm 0.75$. Comparing with the

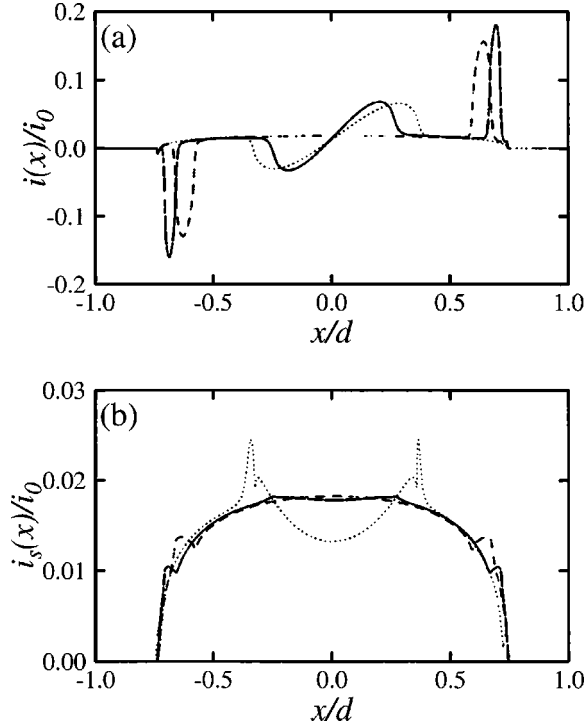


FIG. 9. (a) The current densities $i(x)$ in units of $i_0 = eE_0/2\pi\hbar d$ plotted for the occupation numbers $\nu(0) = 2.05$ (dotted), 3.0 (dashed), and 4.05 (solid) with the same parameters as in Fig. 7. (b) The symmetrized current density drawn for each of these occupation numbers.

electron density for zero current, the lack of charges at the left edge makes a dip at $x \sim -0.75$ while a peak appears at $x \sim 0.75$ by excess charges. Around the center of the Hall bar as well as near the edges, the potential distribution depends strongly on the occupation number. When the chemical potential is pinned at the Landau level around the center [$\nu(0) = 3.0$ and 5.0], the potential distribution varies smoothly across the Hall bar due to a wide compressible region. However, at the magnetic fields such as $\nu(0) = 2.0$ and 4.0 , we find a nonlinear shape of the potential resulting from poor screening in the incompressible regions. Very similar behavior to this has been observed by Knott *et al.*⁸ who measured the voltage drop using a contactless method based on the electro-optical effect. By varying the magnetic field they observed that in a plateau region of the Hall voltage [i.e., $\nu(0)$ is about 2.0] the potential shows nonlinear behavior across the Hall bar while in the transition region the potential drop was found to be distributed linearly. However, the measured potentials do not show any potential peaks caused by the incompressible strips as well as the small peaks near the edges resulting from the charge transfer. We think that the absence of the detailed structure in the induced potential is due to low resolution in the experiment.

Under a given equilibrium current, the effect of the magnetic field on the induced potential is found to become smaller as the temperature increases. In Fig. 8(b), we show the induced potential for various temperatures when the occupation number corresponds to $\nu(0) = 4.05$. The reduced screening of electrons with increasing temperature gives rise to a smaller width of the incompressible region and, thus, peaks in the induced potential become smaller. Eventually,

the induced potential shows linear behavior at high temperature ($k_B T/\hbar\omega_c = 0.5$). Besides the linearly varying shape, the induced potential shows very similar behavior to the case of zero current. The variation of the induced potential is still of the order of $\hbar\omega_c$ around the center of the Hall bar as the temperature is changed from $k_B T/\hbar\omega_c = 0.005$ – 0.5 .

We also examine the current density which is defined as,

$$i(x) = \frac{l_m^2}{\hbar} \frac{\partial U(x)}{\partial x} n(x), \quad I = \int_{-d}^d i(x) dx, \quad (18)$$

for various temperatures and occupation numbers. Figure 9(a) shows, at very low temperature, the current densities $i(x)$ for the occupation numbers, $\nu(0) = 2.05, 3.0,$ and 4.05 for a small drift velocity $v = 0.2v_0$. The current densities show a broad distribution modulated with large peaks which appear in the incompressible region. In the incompressible region, the quantity $\partial U(x)/\partial x$ gives rise to a large value (i.e., large diamagnetic current), however, the net contribution to the current vanishes due to the opposing signs at opposite edges. Thus, neglecting diamagnetic currents in the incompressible regions, we find that the current densities are broadly distributed over the region occupied by electrons. In Fig. 9(b), we show a symmetrized current density $i_s(x) = [i(x - x_c) + i(x_c - x)]/2$, where x_c is the center of mass of the electron distribution. The calculated result is rather similar to that obtained by Pfannkuche and Hajdu,⁴ however, contradictory to the prediction of Chang¹³ that the current can flow only along the incompressible strips.

For a positive v which means the current flows along the positive y direction, the electron distribution is shifted to the positive x direction due to the Lorentz force. An additional shift of the electron density is possible by the gate potential V_R . Under a small applied current, we can obtain a nearly symmetric electron distribution ($a = b$) by adjusting the gate voltage V_R . From our numerical results, we find that the electron density $n_s(x)$ with $a = b$ is obtained when the applied current and magnetic field are related to the gate voltage V_R through,

$$V_R = -\gamma \frac{\pi\hbar v d}{e l_m^2} = -\frac{\pi\gamma}{2} R_H I, \quad (19)$$

where $R_H = B/e\bar{n}$ and γ is a numerical constant depending on a_0/d , \bar{n}/n_0 and $k_B T/E_0$. For various sets of \bar{n}/n_0 and a_0/d , we find that our results are well fitted by the above equation with $\gamma = 2d/\pi b$ at the temperature $k_B T/\hbar\omega_c = 0.005$, leading to $bV_R/d = -R_H I$, where $2b$ is the width of the area occupied by electrons.

V. SUMMARY

In conclusion, we have investigated the local potential, electron, and current distributions of the idealized two-dimensional Hall bar geometry within the Thomas-Fermi approximation. By solving a self-consistent problem, the formation of compressible and incompressible regions is examined for various parameters; current (I), magnetic field (B), gate potential (V_R), average electron density (\bar{n}), bare screening length (a_0), and temperature (T). For zero current, our results are compared with those of CMS. At very low

temperature and small screening length, the analytic expression of CMS is in good agreement with our results. For larger screening length, however, we find that the widths of the central incompressible strips show smaller values than those by CMS. Considering the effect of the gate voltage $V_R \neq 0$, a drastic change is found in the central incompressible regions, which reflects the variation of the electron distribution. With an increase of temperature, the slope of the potential in the compressible region is found to increase proportional to temperature while the width of the incompressible region decreases. As a result, when the temperature is varied largely, the potential variation around the center of the Hall bar is found to be of order of $\hbar \omega_c$ and should be measurable experimentally. Using a generalized equilibrium density operator, we describe a nondissipative equilibrium current flowing along the Hall bar. Under a small nondissipative current, we have shown the calculated electrostatic potential and electron density as well as the current distribution. Since

the applied current transfers electrons from one side of the Hall bar to the other due to the Lorentz force, the resulting potential distribution is drastically different from the case of zero current. However, the shape of the electron distribution is found to be nearly invariant while its center of mass is shifted. We find that the shift of the electron distribution can be canceled by applying a suitable gate voltage. The current density shows a broad distribution modulated with large peaks which appear in the incompressible region. Neglecting diamagnetic currents, however, we find that the current densities are distributed over the whole region occupied by electrons without any preferred region.

ACKNOWLEDGMENTS

We thank U. Gossmann and Dr. D. Pfannkuche for helpful discussions.

-
- ¹J. Hajdu and U. Gummich, *Solid State Commun.* **52**, 985 (1984).
²D. B. Chklovskii, B. I. Shklovskii, and L. I. Glazman, *Phys. Rev. B* **46**, 4026 (1992).
³K. Lier and R. R. Gerhardt, *Phys. Rev. B* **50**, 7757 (1994).
⁴D. Pfannkuche and J. Hajdu, *Phys. Rev. B* **46**, 7032 (1992).
⁵P. F. Fontein *et al.*, *Phys. Rev. B* **43**, 12 090 (1991).
⁶N. B. Zhitenev *et al.*, *Phys. Rev. Lett.* **71**, 2292 (1993).
⁷W. Dietsche, K. von Klitzing, and K. Ploog, *Surf. Sci.* **361**, 289 (1996).
⁸R. Knott *et al.*, *Semicond. Sci. Technol.* **10**, 117 (1995).
⁹G. Ernst *et al.*, *Phys. Rev. Lett.* **77**, 4245 (1996).
¹⁰D. B. Chklovskii, K. A. Matveev, and B. I. Shklovskii, *Phys. Rev. B* **47**, 12 605 (1993).
¹¹U. Wulf, V. Gudmundsson, and R. R. Gerhardt, *Phys. Rev. B* **38**, 4218 (1988).
¹²Y. Wei and J. Weis (unpublished).
¹³A. M. Chang, *Solid State Commun.* **74**, 871 (1990).
¹⁴M. Büttiker, *IBM J. Res. Dev.* **32**, 317 (1988).
¹⁵C. W. J. Beenakker, *Phys. Rev. Lett.* **64**, 216 (1990).
¹⁶L. I. Glazman and I. A. Larkin, *Semicond. Sci. Technol.* **6**, 32 (1991).